Polskie Towarzystwo Materiałów Kompozytowych
Polish Society of Composite Materials

25: 4 (2025) 252–259

COMPOSITES THEORY AND PRACTICE

ISSN (online): 2299-128X

Priyadarshini Shivani Sahoo, Priyabrata Pattanaik, Satyanarayan Bhuyan, Jagadish Chandra Padhi*

Faculty of Engineering and Technology, Siksha 'O' Anusandhan Deemed to be University, Bhubaneswar 751030, India
* *Correspondence:* jagadishpadhi@soa.ac.in

Received (Otrzymano) 19.10.2025
Published on-line (Opublikowano) 31.12.2025

COMPREHENSIVE STUDY ON FREQUENCY-TEMPERATURE DEPENDENT ELECTRICAL PROPERTIES OF SYNTHESIZED $Bi_{1.7}LA_{0.3}NI_2FE_2O_8$ CERAMIC FOR ELECTRONICS APPLICATIONS

https://doi.org/10.62753/ctp.2025.03.4.4

In order to distinguish the fabricated lanthanum doped bismuth-nickel ferrite perovskite oxide material ($Bi_{1.7}La_{0.3}Ni_2Fe_2O_8$) as a competitive ferroelectric component, the material's ferroelectric and electrical properties were investigated. Complex impedance spectroscopy, electric modulus spectroscopy, P-E hysteresis loop measurement, capacitance-temperature measurement, FTIR absorption spectroscopy and UV-Visible spectroscopy were carried out to delineate its multifunctional properties. This La substituted material is characterized by excellent frequency-temperature stability, a semiconducting nature, non-Debye thermal relaxation, ferroelectric property (polarization 0.4μC/cm^2), temperature dependent capacitance maximum sensitivity (58.7nF/°C) and a stable optical band gap (~3.32 eV), which are the major attributes of this ceramic to substantiate it as a promising ferroelectric entity for advanced technological applications.

Keywords: $Bi_{1.7}La_{0.3}Ni_2Fe_2O_8$ ceramic, multifunctional characterization, device performance

INTRODUCTION

The creation of sophisticated mixed metal oxide-based ceramic materials has an enormous impact on how electronic appliances are developed in the current technical breakthrough of ceramic manufacturing [1–2]. The exceptional electrical and magnetic properties of metal oxide-based complex perovskite ceramic materials, along with their physico-chemical stability and thermal-electrical-mechanical resistance, make them superior to other materials in industrial and research applications such as capacitors, data storage devices, dielectric substrates, energy harvesters, phase shifters, actuators, filters, transducers, sensors, photo-catalysis and spintronics [3–7]. Among other ceramics, mixed metal oxide-based bismuth ferrite $BiFeO_3$, has been considered as a potential entry into the electronics application field because of its many striking and varied properties, featuring excellent dielectric strength, insignificant dielectric losses, temperature-independent resonant frequency, and wide frequency dispersion [8]. Even though it has numerous positive aspects, its inherent issues like high discharge current, lower magneto-electric responsiveness, and dynamic distortion accompanied by tangential loss, may alter the ways the device functions [9]. Thus, there has been an ongoing endeavor to achieve better electrical properties of $BiFeO_3$ through the incorporation of other atoms / additional elements on either the A or B sites, which has been assumed to

be another successful approach to changing the properties. Prior research suggests that the emergence of secondary phases may be diminished by substituting isovalent elements or atoms at the Bi-sites. On the other hand, isovalent substitution at the Fe-site modifies its magnetic characteristics without significantly changing its ferroelectric activity [10–12]. Conversely, the substitution of a different ionic charge than the atom it replaces at the Bi-site or Fe-site creates more oxygen vacancies, which ultimately improves the electrical properties [13]. Moreover, it has been reported that partial substitution with ferromagnetic substances like nickel (Ni) in $BiFeO_3$ is highly beneficial since it modifies the dielectric response, making promising materials for device applications because Ni^{2+} has a similar ionic radius to Fe^{3+}. The incorporation of nickel in the Fe-site can lessen leakage by lowering oxygen vacancies and enhances the piezoelectric, ferromagnetic and ferroelectric properties [14–17]. Even though there have been studies on rare earth substituted bismuth ferrite based complex ceramics [18–19], there has not yet been any thorough research on the existence of rare earth lanthanum with the incorporation of an equal proportion of nickel at the B-site (Fe-site) without altering the A-site (Bi-site). The equal proportions of Ni and Fe occupying the Fe-site behave as a double perovskite-like derivative of $BiFeO_3$, which may alter the dielectric properties due to the following exchange: (Fe–O–Fe → Fe–O–Ni / Ni–O–Ni). The substitutions of La^{3+} at the Bi^{3+} site can suppress oxygen vacancies and enhance phase purity, while Ni^{2+} at the Fe^{3+} site can strengthen magnetic exchange interactions. The combined effect can result in enhanced structural stability and dielectric properties. Thus, there is a great deal of interest in lanthanum doped bismuth-nickel ferrite perovskite oxide-based lead-free dielectric components, which offer an environmentally friendly alternative for use in multifunctional electronic device applications.

In the present study, a lanthanum (La^{3+}) substituted bismuth mixed metal oxide-based ceramic $Bi_{2-x}La_xNi_2Fe_2O_8$ with x = 0.3 was produced from Bi_2O_3, Fe_2O_3, La_2O_3 and NiO utilizing a new step-sintering procedure for solid-state mixed oxides process for raw materials. Measurements and thorough analysis were conducted to reveal the desired electrical properties in order to validate the processed material as a good ferroelectric element for high-tech electronic uses.

PRODUCTION AND CHARACTERIZATION

The ceramic sample, $Bi_{1.9}La_{0.1}Ni_2Fe_2O_8$, was prepared using a traditional solid-state reaction process with bismuth (III) oxide (Bi_2O_3), lanthanum (III) oxide (La_2O_3), nickel (II) oxide (NiO), and ferric oxide (Fe_2O_3). The powders used were of analytical quality (> 99.9 % pure) from Pvt. Ltd. Loba Chemicals, India. To make a dielectric sample, the raw oxide particles were ground both wet and dry. After the powder was calcined (heated to 800°C), a polyvinyl alcohol binder was added and combined well to make granules. This mixture was then utilized to make discs with dimensions 10 mm × 2 mm by employing a uniaxial hydraulic press that applies a compaction pressure of 5×10^6 N/m². After that, the discs underwent heating to 850°C for four hours on an alumina boat. Silver paste was used as the electrodes on both sides of the sample so that different electrical measurements could be taken. Then, using an NF Corporation LCR meter ZM-2376, a number of properties were measured, such as impedance, and conductivity between 35 and 400°C and 1–1000 kHz.

RESULTS AND DISCUSSION

Impedance spectrum analysis

At different temperatures, the electrical properties that depend on the frequency of the reactive (Z'') and resistive (Z') modules of the $Bi_{1.7}La_{0.3}Ni_2Fe_2O_8$ ceramic are shown in Fig. 1(a)–(b). The Z' value was observed to decrease with increasing frequency at all the selected temperatures. Temperature affects the Z' value in the spectrum of low frequencies, but these curves coincide in the high frequency range. The resistive response is dominated by slow moving charge carriers,

space charge accumulation, grain boundaries and interfacial polarization. The Maxwell-Wagner interfacial polarization theory states that the polarization effects are the strongest at low frequencies and gradually decline as charge carriers lose their capacity to effectively collect and separate, causing the resistance to decrease with increasing frequency [20].

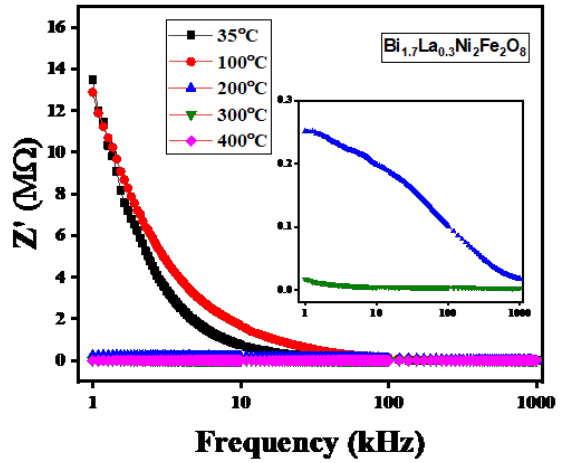

a)

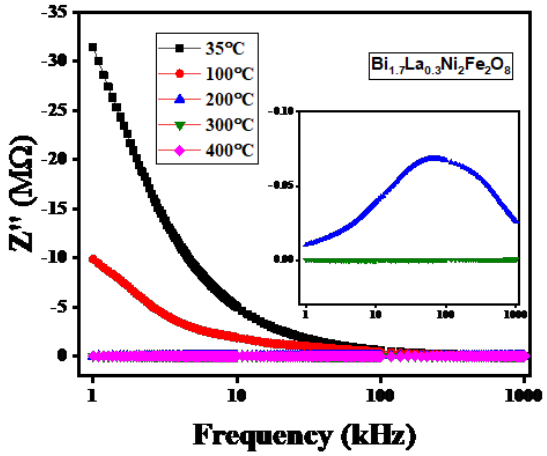

b)

Fig. 1. Frequency-dependent complex impedance spectrum of Bi1.7La0.3Ni2Fe2O8 at specific temperatures, delineating (a) resistive component and (b) reactive component

This further reveal that the oxygen vacancies of the produced ceramic sample enhanced the frequency-dependent relaxation properties. The Z" values coincide with each another at upper frequencies. It is apparent that this material's relaxation process only works at high temperatures, and it could be brought on by the prevalence of immobile flaws in the sample [20].

Analysis of Nyquist diagrams

Figure 2 shows the Z' vs Z" (Nyquist plot) of the synthesized $Bi_{1.7}La_{0.3}Ni_2Fe_2O_8$ at several temperatures and frequencies. The impedance characteristics of the specimen are shown by semi-circular arcs that build up and their succession (diameter and position) changes with temperature. In the Nyquist simulation, several semi-circular curvatures demonstrate how the grain, grain border, and electrode effect work together [21]. The presence of sole arcs indicates that electrical progressions of the material are affected by the grains.

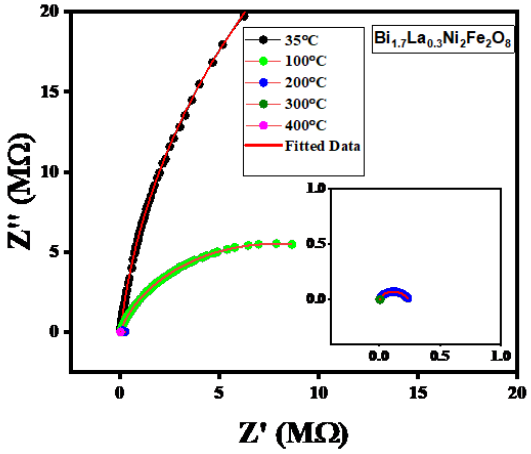

Fig. 2. Nyquist plot at selected temperatures of Bi1.7La0. 3Ni2Fe2O8

Figure of merit analysis

To measure the equilibrium between dielectric storage and loss, the figure of merit (FoM) for $Bi_{1.7}La_{0.3}Ni_2Fe_2O_8$ was calculated as FoM = ε′/tanδ at a set of excitation frequencies (1 kHz-1 MHz). FoM increases at lower and intermediate frequencies (about 1–100 kHz), the most as the temperature grows, as elucidated in Fig. 3(a)–(b). This is because in the near-edge regime, ε′ grew faster than tanδ due to thermally triggered interfacial polarization and small-polaron hopping. Because slow polarization mechanisms cannot track the field at higher frequencies (about 1 MHz), only rapid intrinsic dipoles contribute, and FoM is relatively low and practically temperature-independent at these higher frequencies. Consistent with $\tan\delta = \sigma_{ac}/(\omega\varepsilon_o\varepsilon')$, a plateau or minor

decline could happen at the highest temperatures when conduction losses take over. On the whole, $Bi_{1.7}La_{0.3}Ni_2Fe_2O_8$ has a practical working window where FoM is at its maximum at lower and intermediate frequencies before leakage-driven loss kicks in, and while running at high frequencies, thermal stability improved, but FoM decreased.

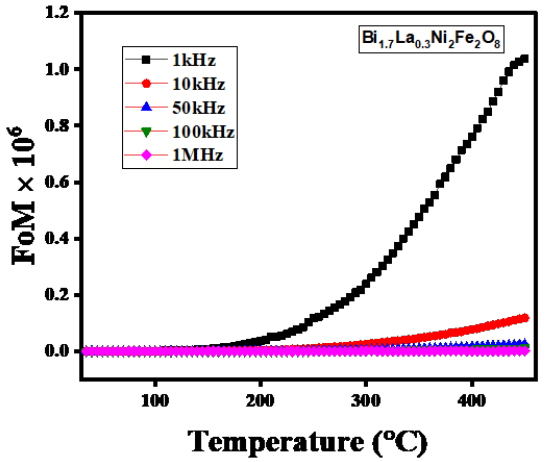

a)

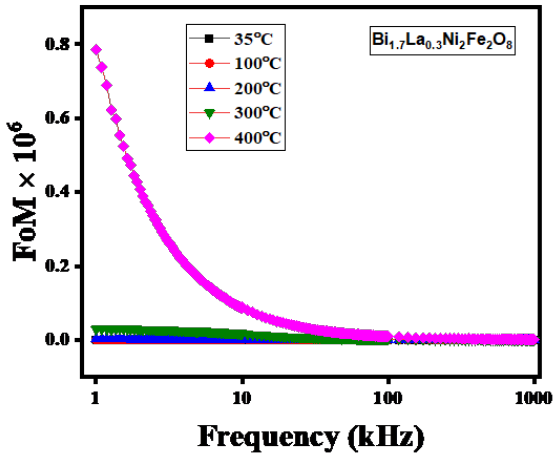

b)

Fig. 3. Characteristics of figure of merit (a) variation with frequency (b) with temperature

Conductivity spectrum and temperature dependency analysis

The AC conductivity of the produced ceramics that depends on frequency and temperature properties is shown in Fig. 4(a) and (b), respectively. The following equation yields the AC electrical conductivity:

$$\sigma_{ac} = 2\pi f \varepsilon_o \varepsilon_r \tan\delta \quad (1)$$

The frequency dependent curves converging at high frequencies and proceeding in the same direction are signs of conductivity dispersion. The figure illustrates conductivity, which is characterized by an increase in frequency resulting from the inhibition of charge accumulation [22]. The space charge and neighboring sites may cause cation distortion, which would explain the rise in conductivity. A decrease in AC conductivity σ_{ac} is observed with a rise in temperature. The enhancement in σ_{ac} beyond 200°C simply reflects the thermally stimulated small-polaron hopping and oxygen vacancy driven charge release, which lessens resistivity with growth of temperature, and therefore manifests the semiconducting NTCR behavior (negative temperature coefficient of resistance). Apart from this, activation energy E_a was calculated for the sample, which is known to be a crucial component in doping, defect analysis, and defining electrical characteristics like conductivity. E_a is ascertained by finding the slope of the linear parts of the temperature-dependent AC conductivity curve. Following that, the activation energies (E_a) are calculated using the Arrhenius equation [23]:

$$\sigma_{ac} = \sigma_0 \exp(-E_a / K_B T) \quad (2)$$

The sample underwent multiple conduction processes because the slope values change in different temperature zones. At the frequencies of 1 KHz, 10 KHz, 50 KHz, 100 KHz, and 1 MHz, the sample's E_a values are 0.357 eV, 0.327 eV, 0.326 eV, 0.310 eV, and 0.281 eV, respectively. Based on this information, it appears that the sample's activation energy falls with rising temperature and frequency because of increased small-polaron/defect-dipole hopping and Maxwell-Wagner interfacial polarization. A higher temperature lowers the grain-boundary barriers and increases carrier delocalization, whereas a higher frequency enables the dipoles to follow the alternating field, resulting in localized hopping with reduced energy barriers. As a result, the effective activation energy falls.

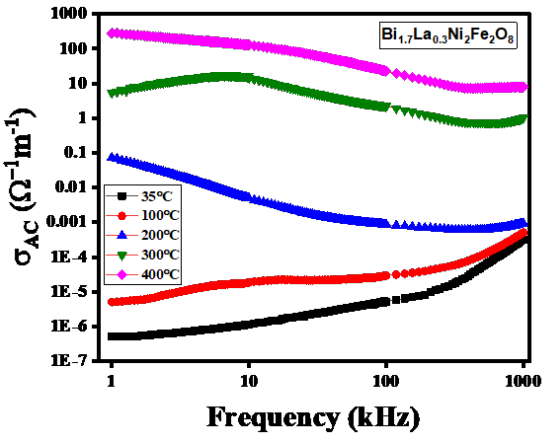

Fig. 4(a). Frequency dependent AC conductivity spectrum of Bi1.7La0.3Ni2Fe2O8 at selected temperatures

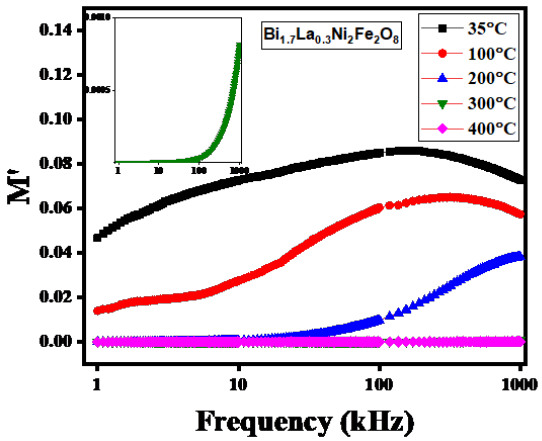

a)

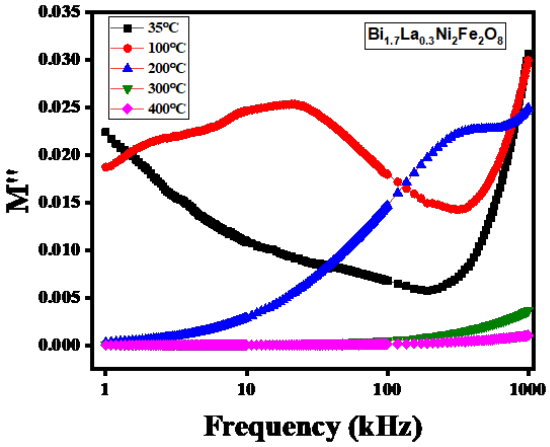

b)

Fig. 5. Characteristics of (a) real part- M' (b) imaginary part-M'' of complex modulus

Electrical modulus spectrum

The electrical modulus is simply the inverse of the complex permittivity and is used to suppress electrode polarization, interfacial polarization and isolate bulk relaxation mechanisms. Additionally, it aids in the detection of various relaxation times and imperfections like grain boundaries. It consists of both fictional and actual parts. Figure 5(a) and (b) illustrate how the real portion M' and imaginary part M'' of complex electric modulus M* vary with frequency for the $Bi_{1.7}La_{0.3}Ni_2Fe_2O_8$ sample under various temperatures. The real part of electric modulus M' goes to zero when the temperature is high and the frequency is low. Additionally, the curves tend to line up at greater temperatures. Conduction phenomena and the possibility of charge carrier mobility having a restricted range could be the root causes of this phenomenon [23]. It demonstrates how the lack of restorative force limits the movement of charge when an electric field is stable. By inverting the permittivity, low-frequency space-charge contributions are compressed and the bulk relaxation processes appear as well-defined peaks in M' versus frequency plots. The fact that there are peaks at higher frequencies and temperatures implies that thermal triggers are responsible for dielectric relaxation, which is typically controlled by the hopping mechanism of charge particles. Figure 5(a) implies that an increase in charge carrier mobility facilitates a decrease in relaxation time. Non-Debye type behaviour or multiple relaxation processes are indicated by asymmetrical peak widening [23].

Ferroelectric hysteresis (P-E loop)

The hysteresis loop shows how the polarization (*P*) changes with the electric field (E) at the frequency of 50 Hz. Figure 6 shows the room temperature ferroelectric hysteresis loop of $Bi_{1.7}La_{0.3}Ni_2Fe_2O_8$. The sample demonstrates the overarching tendency of the ferroelectric hysteresis loop, indicating the existence of ferroelectric properties. The sample's leftover polarization value is 0.4 $\mu C/cm^2$. Under the applied electric field, the P-E loop of the sample appears to be unsaturated, indicating field dependent polarization and significant dielectric tunability. The pragmatic polarization response reflects the sample's receptive dielectric behavior that is proper for capacitive sensing.

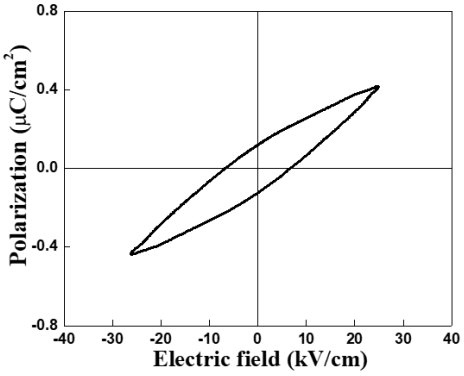

Fig. 6. P-E loop of Bi1.7La0.3Ni2Fe2O8ceramic

Temperature dependent capacitance sensitivity

Fig. 7 presents the capacitance-temperature relationship of the BNFO ceramic. The capacitance exhibits a linear pattern as the temperature goes up. The sensitivity is determined using the formula:

$$S(pF/°C) = (C_{fT}\text{-}C_{iT})/(T_f\text{-}T_i) \quad (3)$$

The linear fit of the curve indicates that the sensitivity is 2.048 nF/°C at low temperatures (up to 230°C) and 58.7 nF/°C at higher temperatures. This is because the relative permittivity (ε_r) rises with temperature below the Curie transition temperature (T_c). The Lydanne-Sachs-Teller connection explains the changes in both longitudinal and transverse optical phonons with temperature, which increases capacitance [23].

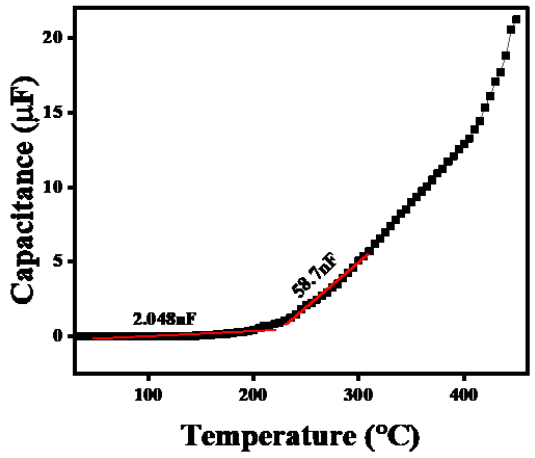

Fig. 7. Temperature-dependent Bi1.7La0.3Ni2Fe2O8 ceramic components' capacitive characteristic

Fourier transform infrared absorption band spectrum

The FTIR spectrum of the produced $Bi_{1.7}La_{0.3}Ni_2Fe_2O_8$ sample, displayed in Fig. 8, shows characteristic absorption bands that demonstrate the existence of residual surface functional groups as well as metal-oxygen interactions.

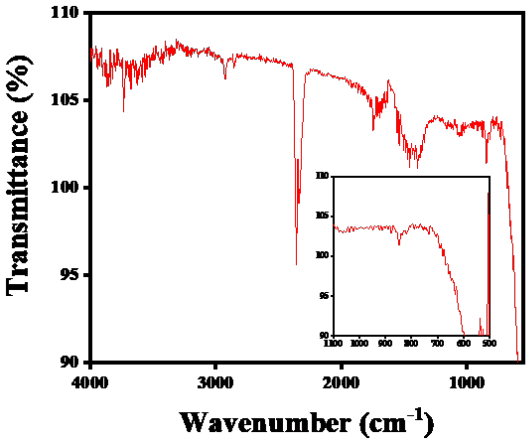

Fig. 8. FTIR spectrum of Bi1.7La0.3Ni2Fe2O8 ceramic

The large peaks observed between 3949 and 3648 cm^{-1} are indicative of O–H stretching vibrations, which are induced by adsorbed water and surface hydroxyl groups. The absorption band for 846 cm^{-1} and 669 cm^{-1} resembling M–O stretching vibrations (Bi-O, Fe–O, Ni–O), validates the formation of the metal oxide structure [24]. The outcome is a localized structural deformation that is reflected by slight variations in the Fe-O and Ni-O vibration frequencies. These observations collectively demonstrate that a mixed metal oxide structure has been successfully produced in accordance with the $Bi_{1.7}La_{0.3}Ni_2Fe_2O_8$ formulation.

UV-Visible spectroscopy

UV-Vis is a non-destructive optical technique which was employed to explore the electrical structure of the produced ceramic by measuring the fraction of incident UV visible light that is diffusely reflected [25]. Fig. 9 illustrates the UV-Visible spectra and Tauc plot of the $Bi_{1.7}La_{0.3}Ni_2Fe_2O_8$ ceramic component.

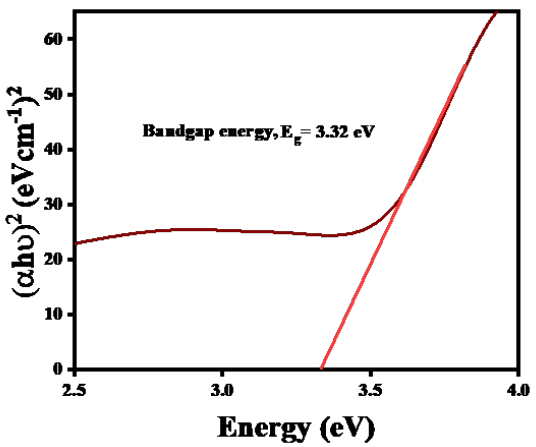

Fig. 9. UV-Visible spectra and Tauc plot of Bi1.7La0.3Ni2Fe2O8 ceramic

The reflectance (R) recorded on oxide ceramics and other strongly scattering media can be transformed into an absorption coefficient. The optical energy band gap can be calculated using the following formula:

$$(\alpha\upsilon h)^n = B(h\upsilon - E_g), \quad (4)$$

where 'n' stands for the electronic transition nature, 'B' for the proportionality constant, 'h' for Planck's constant, 'α' for the absorption constant, and 'E_g' for the band gap energy. For a direct-allowed transition with n=2 and the indirect-allowed transition with n=½, the assessed band gap (E_g) is 3.32 eV. This substantial optical band gap indicates that this ceramic could be used as dielectric substrates for potential applications in data storage devices and electronic circuit packaging. A wide band gap generally corresponds to a low intrinsic carrier concentration, reduced electronic leakage, and enhanced electrical insulation properties that are essential for dielectric substrates operating under high-frequency or high-temperature conditions.

CONCLUSIONS

In this study, a new ceramic substance $Bi_{1.7}La_{0.3}Ni_2Fe_2O_8$ was produced using a solid-state reaction based on a mixed oxides approach. Complex impedance spectroscopy was employed to assess the dielectric properties in relation to temperature and frequency. This material has been validated as an appropriate ferroelectric component for device design by the practical measurement of its optical band gap, absorption band spectra, temperature-dependent frequency dispersion impedance, and capacitive properties. The investigation corroborates the improved dielectric properties, supporting the notion that it may serve as a suitable ceramic material for various sophisticated technological applications like energy storage, optoelectronic, photo-catalytic, multiferroic, and magneto-electric devices.

REFERENCES

[1] K.S. Randhawa, Advanced ceramics in energy storage applications: Batteries to hydrogen energy, J. Energy Storage 98, 113122 (2024).

[2] M. Bhavisha, K. Anjali, S. Aswani, A. Sakthivel, Catalytic applications of perovskites, in Ceramic Catalysts, Elsevier, 19–55 (2023).

[3] S.K. Sourav, S.K. Parida, R.N.P. Choudhary, U. Prasad, Studies of structural, microstructure, dielectric and optical properties of bismuth-based complex perovskite modified bismuth ferrite: $BiFeO_3$–$(Bi_{0.5}Na_{0.25}K_{0.25})(Ti_{0.5}Mn_{0.5})O_3$ ceramics, Trans. Electr. Electron. Mater. 24(5), 434–446 (2023).

[4] H. Esfanddarani, M. Panigrahi, Phytosynthesis of transition (Ni, Fe, Co, Cr, and Mn) metals and their oxide nanoparticles for biomedical applications: a review, J. Mater. Sci. 59(24), 10677–10723 (2024).

[5] S. Masih, N. Sharma, S. Kumar, A. Kaur, S. Middha, P.D. Babu, R. Ghosh, Flexible ceramic composites for magnetic field sensor applications, Ceram. Int. 51(5), 5790–5798 (2025).

[6] R. Muhamma, Y. Iqbal, and Ian M. Reaney, $BaTiO_3$–$Bi(Mg_{2/3}Nb_{1/3})O_3$ ceramics for high temperature capacitor applications, Journal of the American Ceramic Society, 99 (6), 2089-2095 (2016).

[7] G. Catalan, J.F. Scott, Physics and applications of Bismuth Ferrite. Adv Mater. 21:2463–85 (2009).

[8] Z. Sun, J. Wei, T. Yang, M. Xiahou, A. Cao, J. Zhang, Y. Yuanfeng, Y. He, Multifactorial coupling to greatly enhance photocurrent density of $BiFeO_3$-based ferroelectric photovoltaic architectures, J. Mater. Sci.: Mater. Electron. 35(31), 2035 (2024).

[9] S.K. Singh, K. Maruyama, H. Ishiwara, Reduced leakage current in La and Ni codoped $BiFeO_3$ thin films. Appl. Phys Lett. 91:112913–15 (2007)

[10] Dinesh Varshney, Ashwini Kumar, Kavita Verma, Effect of A site and B site doping on structural, thermal, and dielectric properties of BiFeO3 ceramics, Journal of Alloys and Compounds, 509, 33, 8421-8426 (2011).

[11] J. Bielecki , P. Svedlindh, D.T. Tibebu, S. Cai, S.G. Eriksson, L. Borjesson, C.S. Knee Structural and magnetic properties of isovalently substituted multiferroic BiFeO3: insights from Raman spectroscopy. Phys Rev B Condens Matter Phys. 86:184422 (2012).

[12] Jianguo Zhao, Xianghui Zhang, Shijiang Liu, Weiying Zhang, Zhaojun Liu, Effect of Ni substitution on the crystal structure and magnetic properties of BiFeO3, Journal of Alloys and Compounds, 557, 120-123 (2013)

[13] Haiyang Dai, Fengjiao Ye, Zhenping Chen, Tao Li, Dewei Liu, The effect of ion doping at different sites on the structure, defects and multiferroic properties of $BiFeO_3$ ceramics, Journal of Alloys and Compounds, 734, 60-65 (2018)

[14] Tao li, Zhenping Chen, Investigations on the structure, defects, electrical and magnetic properties of Ni-substituted BiFeO3 ceramics' Journal of Materials Science: Materials in Electronics, 27, 11, 11151–11157 (2016)

[15] C. Behera, R.N.P. Choudhary, P.R. Das, Structural and electrical properties of La-modified BiFeO3–BaTiO3 composites. J. Mater. Sci. Mater. Electron. 25, 2086-2095 (2014).

[16] N.K. Mohanty, A.K. Behera, S.K. Satpathy, B. Behera, P. Nayak, Effect of dysprosium substitution on structural and dielectric properties of $BiFeO_3$-$PbTiO_3$ multiferroic composites, Journal of Rare Earths, 33 (6) 639-646 (2015).

[17] S.K. Samal, B. Biswal, M.K. Mallick, R.N.P. Choudhary and S. Bhuyan, Frequency–temperature-dependent electrical properties of fabricated $(Pb_{0.7}Bi_{0.15}Sm_{0.15})(Ti_{0.7}Fe_{0.3})O_3$ capacitive electronic material component, Appl. Phys. A 128, 683 (2022).

[18] A. Kumari, K. Kumari, R.N. Aljawfi, Role of La substitution on structural, optical, and multiferroic properties of BiFeO3 nanoparticles. Appl Nanosci 13, 3161–3180 (2023).

[19] A. Srivastava, A.K. Singh, O.N. Srivastava, H.S. Tewari, K. B. Masood, J. Singh, Magnetic and Dielectric Properties of La and Ni Co-substituted BiFeO3 Nanoceramics, Frontiers in Physics, 8 , (2020)

[20] M. Samet, A. Kallel, A. Serghei, Maxwell-Wagner-Sillars interfacial polarization in dielectric spectra of composite materials: Scaling laws and applications. Journal of Composite Materials, 56, 3197 (2022).

[21] S. Kalingani, S.N. Das, S. Bhuyan, Structural, microstructural, morphological, electrical spectroscopy and optical analysis of lithium–titanium oxide electronic material, Inorg. Chem. Commun. 159, 111731 (2024).

[22] P. Kumar, J.K. Juneja, C. Prakash, K.K. Raina, S. Singh, Effect of Sm on dielectric, ferroelectric and piezoelectric properties of BPTNZ system, Physica B 426, 112–117 (2013).

[23] S. Halder, S. Bhuyan, R.N.P. Choudhary, Structural, dielectric and electrical properties of bismuth magnesium tantalate electronic system, J. Magn. Alloys 7(4), 628–636 (2019).

[24] N. Sakib, F. Nahid, S.F.U. Farhad, N. Khatun, S.S. Islam, M.A. Rayhan, M.D. Hossain, M.N.A. Bitu, S.M. Hoque, M. Al-Mamun, Effects of nickel substitution on structural, magnetic and optical properties of Sillenite bismuth ferrite nanoparticles, Journal of Solid State Chemistry, 340, 125045 (2024)

[25] M.M. Gois, et al., $Bi_{25}FeO_{40}$-Fe_3O_4-Fe_2O_3 composites: synthesis, structural characterization, magnetic and UV–visible photocatalytic properties, J. of Alloys and Compounds 785,598–602 (2019).